Research Article Vol. 58, No. 14 / 10 May 2019 / Applied Optics 3775

applied optics

# 3D mapping of droplet Sauter mean diameter in sprays

Yogeshwar Nath Mishra,[1,*] Matthias Koegl,[1,2] Kevin Baderschneider,[1] Bernhard Hofbeck,[1] Edouard Berrocal,[2,3] Chris Conrad,[1,2] Stefan will,[1,2] and Lars Zigan[1,2]

[1]Lehrstuhl für Technische Thermodynamik (LTT), Friedrich-Alexander-Universität Erlangen-Nürnberg (FAU), 91058 Erlangen, Germany
[2]Erlangen Graduate School in Advanced Optical Technologies, FAU, 91052 Erlangen, Germany
[3]Division of Combustion Physics, Lund University, Box 118, Lund 22100, Sweden
*Corresponding author: yogeshwar.mishra@fau.de

Received 27 February 2019; revised 11 April 2019; accepted 11 April 2019; posted 11 April 2019 (Doc. ID 359857); published 6 May 2019

**In this study, we report on the three-dimensional (3D) characterization of a spray in terms of its droplet Sauter mean diameter (SMD) using the laser-induced fluorescence (LIF)/Mie ratio technique. The spray structure is analyzed for a multi-hole direct-injection spark ignition (DISI) injector. A calibration curve to convert the LIF/Mie ratio to droplet diameter is deduced using LIF/Mie imaging and analysis of single droplets generated by a droplet generator. The DISI spray investigated here is optically sectioned by means of two-phase structured laser illumination planar imaging to suppress the intensity of multiple light scattering from LIF and Mie images prior to their ratio. A series of calibrated LIF/Mie ratio images of spray is then recorded at several depths along the $z$ direction following the light sheet scanning of the spray. The droplet SMD ranges from less than 5 µm up to a maximum of 50 µm in single-shot images. The averaged SMD results (1–30 µm) obtained by using the calibration curve from the droplet generator are compared with measurement results from phase-Doppler anemometry. Finally, a 3D map is reconstructed from the successive 2D layers generated from spray scanning. The resulting 3D representation of the droplet SMD shows a non-symmetric spray structure produced by the studied multi-hole injector, which cannot be resolved by analyzing only one central plane.** 

https://doi.org/10.1364/AO.58.003775

## 1. INTRODUCTION

Droplet size and temperature are among the most important quantities required to optimize or predict the fuel–air mixing in fuel sprays, especially in internal combustion engines [1,2]. One of the most common and reliable methods to measure the size of spherical droplets is phase-Doppler anemometry (PDA) [3–6]. This optical approach, however, is restricted to point measurements, making it very time consuming to obtain measurement over the full three-dimensional spray structure. In addition, a collection of PDA-derived Sauter mean diameter (SMD) allows to acquire only temporally averaged data, and no information on the cyclic variation of single injections is delivered. Because of their optical sectioning capabilities, intensity ratio-based laser sheet imaging approaches such as laser-induced fluorescence (LIF)/Mie ratio [7], exciplex-LIF/Mie ratio [8], Raman/Mie ratio [9], and polarization ratio [10] have been used as various attempts for obtaining 2D maps of droplet size. By now combining those laser sheet imaging approaches with a scanning procedure (e.g., by imaging different successive depths [11] or rotating the spray), averaged 3D maps can be achieved.

The LIF/Mie ratio approach exploits the fluorescence and scattering of light signals generated from dye-doped droplets. The technique was reported for the first time in the year 1993 [12]. Since then, the method has been reported in the literature with different names, such as laser sheet dropsizing (LSD) [13,14], planar droplet sizing (PDS) [15–17], or more generally the LIF/Mie droplet sizing.

In this technique, the LIF and Mie optical signals are, respectively, assumed to be cubic and square, dependent on the droplet diameter $d$ [13–17] in the case of spherical micrometric drops. The ratio of LIF/Mie yields a quantity related to $d_{32}$, popularly known as SMD. To avoid fluorescence from the vapor phase, the method has been used mostly for droplet sizing in different types of non- or poorly evaporating water and fuel sprays. For example, Le Gal *et al.* investigated a pressure-swirl atomizing spray of mineral spirit as fuel, using *p*-Terphenyl as a fluorescent tracer [13]. Jermy and Greenhalgh studied a cooling spray of water (SMD in the range of 15–20 µm) using sodium salicylate dye [15]. Stojkovic and Sick characterized a gasoline fuel injector using iso-octane as fuel and 3-pentanone as LIF tracer [18]. The SMD of self-fluorescent unleaded gasoline sprays generated from a gasoline direct injection (GDI) injector were measured in the range 5–40 µm [19]. Domann and Hardalupas reported SMD

mapping in a spray generated by a pressure swirl atomizer in a liquid-fueled burner [17]. Jin *et al.* and Boretti *et al.* investigated air-assisted direct-injection spark ignition (DISI) spray using self-fluorescent standard unleaded petrol fuel [20,21]. Storch *et al.* [22] and Koegl *et al.* [23] used eosin dye as LIF tracer for LIF/Mie droplet sizing in ethanol DISI spray because of its high quantum yield of ~0.68.

The process to extract droplet SMD from the LIF/Mie technique appears straightforward; however, it works only if some conditions are met. For example, the first step is the validation of volumetric $d^3$ and surface $d^2$ dependence of the LIF and Mie signals, respectively. Several numerical and experimental studies have been reported over the years, and it has been found that dye concentration and detection angles are the two major parameters influencing the $d^3$ and $d^2$ relations [16,24–28]. In addition to those effects, a very important issue typically associated with image ratio techniques is the contribution of the light intensity generated from multiple light scattering occurring in dense droplet clouds, which was investigated numerically by Berrocal *et al.* [29] and Stepowski *et al.* [30] as well as experimentally by Powell *et al.* [31]. In 2008, the multiple scattering issues were successfully addressed by combining structured illumination with light sheet imaging by Berrocal and co-workers [32,33], a technique known as structured laser illumination planar imaging (SLIPI). In their subsequent work, the authors demonstrated the capability of the technique on diesel sprays [34], hollow-cone water sprays [35,36], and recently on ethanol/butanol DISI sprays [23]. In another recent study, Kulkarni *et al.* performed SLIPI-LIF/Mie measurements in an air-blast atomizing spray [37].

The accuracy of SMD measurements from LIF/Mie ratios is also governed by the calibration procedure. The majority of calibration schemes are made using PDA measurements, while a few calibration approaches are reported that use a monodisperse droplet generator [38]. Calibration with a monodisperse droplet is preferred because droplets are recorded and evaluated identically to the LIF/Mie ratio scheme (see details in Section 2B). However, the drawback lies in generation and evaluation of droplets of different size classes in great numbers. Droplet generators had been utilized for producing mostly droplets ≥ 50 μm until recently, when single droplets in diameter range of 21–50 μm could be repeatedly produced using a droplet generator utilizing a flow-focusing technique [39].

In a recent paper, Koegl *et al.* [40] systematically investigated the LIF and Mie signal dependencies on $d$ in eosin dye-doped single microscopic ethanol droplets in the size range of 21–60 μm. The incident laser energy, dye concentration, and liquid temperature were examined as the function of LIF/Mie ratio. A calibration curve was successfully deduced from single microscopic droplet analysis, which was then implemented for instantaneous 2D mapping of SMD in ethanol DISI sprays.

In this paper, we extend the study by Koegl *et al.* [40] for the generation of series of 2D SMD sections and the global 3D reconstruction of the droplet distribution of an ethanol DISI spray generated by a multi-hole injector. The experimental investigation is as follows: (i) the LIF/Mie ratio of single microscopic droplets is described in brief for extracting a relation between the signal ratio and droplet diameters. (ii) For the spray investigations, a two-phase SLIPI (2p-SLIPI) approach is combined with LIF/Mie droplet sizing so that the intensity of multiple light scattering from both LIF and Mie signals is suppressed prior to LIF/Mie ratio. (iii) The combined 2p-SLIPI-LIF/Mie approach is implemented with light sheet scanning to intersect the DISI spray in several layers (2D) like "bread slicing." (iv) The calibration deduced from single droplet investigation in (i) is utilized for converting all the 2D layers of LIF/Mie ratio in droplet absolute SMD. (v) The 2D SMD maps obtained in (iv) are compared with droplet SMD measured from the PDA system. (vi) By means of coupling all the 2D layers of droplet SMD maps, a global 3D measurement map of droplet SMD is reconstructed. Finally, 3D SMD maps of droplet SMD and their corresponding coefficient of variation maps are compared.

## 2. PLANAR DROPLET SIZING IN SPRAYS

### A. Description of LIF/Mie Droplet Sizing Approach

As previously mentioned, the method assumes that the fluorescence signal $I_{\mathrm{LIF}}$ and the Mie scattering signal $I_{\mathrm{Mie}}$ generated from spherical liquid droplets are proportional to the droplet volume ($\sim d^3$) or its surface area ($\sim d^2$), respectively. To make this assumption valid, three important conditions must be fulfilled: first, the droplets must be spherical. Second, no fluorescence must be generated from the gas phase. Third, all photons reaching the camera should have experienced only one scattering event prior to detection. If these three main conditions are respected, the resulting intensity ratio $R_{\mathrm{LIF/Mie}}$ is proportional to the droplet SMD, i.e.,

$$R_{\frac{\mathrm{LIF}}{\mathrm{Mie}}} = \frac{I_{\mathrm{LIF}}}{I_{\mathrm{Mie}}} = \frac{K_{\mathrm{LIF}}}{K_{\mathrm{Mie}}} \cdot \frac{\sum_{i=0}^{n} N_i \cdot d_i^3}{\sum_{i=0}^{n} N_i \cdot d_i^2} = K \cdot \mathrm{SMD}, \quad (1)$$

where $K_{\mathrm{LIF}}$ and $K_{\mathrm{Mie}}$ are coefficients related to dye concentration, laser power, signal collection angle, detector response, scattering efficiency, etc. Here, $K$ equals the ratio of $K_{\mathrm{LIF}}/K_{\mathrm{Mie}}$ and corresponds to a curve that is experimentally deduced after calibration. The calibration procedure is usually performed using a PDA instrument that locally provides SMD data [15] or a monodisperse droplet generator, where droplets of known and constant size can be generated [19].

### B. Calibration of LIF/Mie Ratio

The PDA-based calibration of LIF/Mie ratio is straightforward for regions where the PDA probe volume coincides with the plane of the laser sheet [36]. In PDA, when individual drops pass through the probe during an interval, consequently, the number and diameter distribution of all the drops are registered. Using this distribution, the corresponding SMD and other mean diameters can be calculated as given in [41]. Therefore, the PDA measurement is time averaged and sensitive to the number of drops passing through a cross section (particle flux). Opposite to it, the LIF/Mie ratio is deduced from a spatial distribution, when a collection of drops occupies a given measurement volume or voxel of the recorded image.

The calibration approach based on using a droplet generator presents the advantage that the droplet size is known and does not rely on the use of another optical technique. In addition, the approach can be used, for Le Gal *et al.* have reported

calibration of LIF/Mie ratio from the individual droplets produced from the droplet generator in the diameter range of 50–180 μm [13]. Park *et al.* have demonstrated microscopic LIF/Mie ratio calibration from the droplets produced in the range of 50–300 μm [19]. Chen *et al.* have used a mono-sized droplet generator to produce droplet sizes in the range of 200–1000 μm to calibrate LIF/Mie ratio in ethanol DISI sprays [42]. Recently, Koegl *et al.* have performed the calibration of SLIPI-LIF/Mie ratio using the droplet of ethanol produced in the diameter range of 21–60 μm [40]. This droplet size range is particularly relevant for sprays used in combustion applications. Therefore, in this paper, the calibration process of SLIPI-LIF/Mie ratio as proposed in [40] is applied for 2D and 3D droplet sizing.

## 3. EXPERIMENTAL SETUP

The optical setup for the analysis of single droplets in terms of LIF and Mie optical signals is given in Fig. 1. The procedure is described in detail in [40], and only a brief explanation is given here for clarity. Ethanol droplets are produced in the diameter range of 21–65 μm using a flow-focusing monodisperse droplet generator, made by MSP Corp. (Type 1530). The eosin-Y dye (Sigma Aldrich) is used as a fluorescence tracer at a concentration of 0.5% by volume. The dye is excited at 532 nm wavelength from an Nd:YAG-pulsed laser cluster (Thales, France) of the top hat beam profile with a light sheet of dimensions

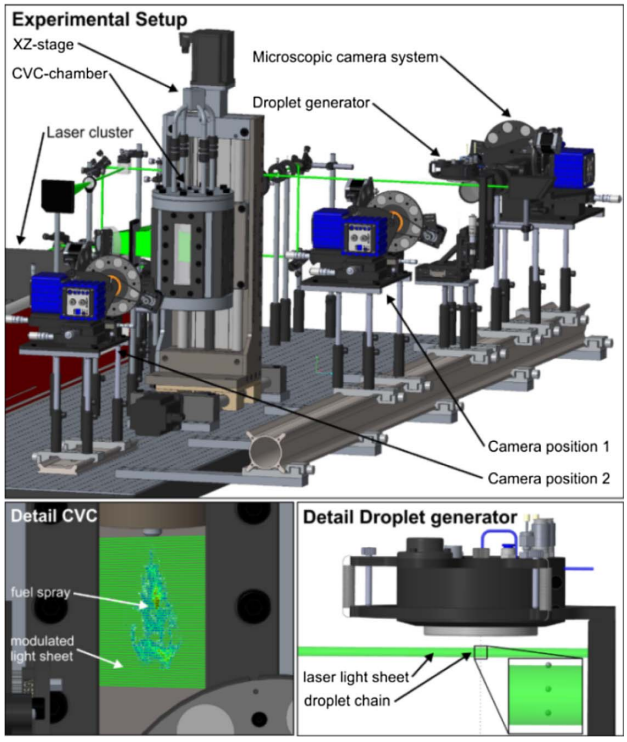


**Fig. 1.** Experimental setup consists of a constant volume chamber (CVC) connected to a translation stage, 2p-SLIPI setup, and a droplet generator. Detailed CVC (bottom left) shows fuel spray illuminated with modulated light sheet of 2p-SLIPI. Detailed droplet generator (bottom right) image shows laser light sheet illuminating droplet chain. The detection consists of the beam splitters, camera objective, LIF and Mie optical filters, and two identical sCMOS cameras.

15 mm in height and approximately 0.7 mm in thickness. The time duration of each pulse is on the order of 6 ns with a repetition rate of 10 Hz. The generated fluorescence signal shows its emission peak at around 550 nm. The fluorescence and Mie scattered light signals are simultaneously recorded using microscopic and macroscopic imaging setups. Throughout the experiments, the laser power and dye concentration are fixed such that the fluorescence signal is kept in the linear regime, which is reported in [40].

The microscopic imaging setup is equipped with a long-range microscope (Infinity, model K2 DistaMax), two identical sCMOS cameras (LaVision GmbH, Germany), two optical filters, and one cube beam splitter (Edmund Optics, UK). The beam cube splits the original signal into a 70% transmission part (towards the LIF camera) and a 30% reflection part (towards the Mie camera). A notch filter with 532 nm central wavelength and 17 nm full width at half maximum (FWHM) is used in front of the LIF camera sensor to exclude the 532 nm excitation wavelength while preserving most of the fluorescence intensity in the spectral range of 540–680 nm. Similarly, a laser line filter with a central wavelength of 532 nm and 1 nm FWHM is used in front of the Mie camera sensor to collect only the Mie signal while rejecting any fluorescence signal. Each recorded image with the two cameras corresponds to 2560 × 2160 pixels. The selected region of interest is equal to 0.71 mm × 0.60 mm with a pixel resolution of 3.63 pixels per μm. The macroscopic imaging setup is equipped with a 135 mm objective (Pentagon 2.8/135), while the cameras, optical filters, and beam cube are identical to the microscopic imaging system. The pixel resolution is 0.15 pixels per μm.

The ethanol DISI sprays are investigated in a constant volume chamber (CVC) using the 2p-SLIPI optical setup [22]. Two additional laser pulses of 532 nm wavelengths (with a top hat beam profile) from the Thales laser cluster are utilized for 2p-SLIPI. The time duration of each pulse is 6 ns with a repetition rate of 10 Hz. The incident sheet has a height of ∼90 mm and thickness of ∼500 μm. The structured patterns are realized using a transmission Ronchi grating (Serial No. 40-16, Applied Image Inc., USA) of spatial frequency of four line pairs/mm. The grating is selected such that modulation depth of the line patterns is preserved over a large pixel area. Identical to the macroscopic LIF/Mie setup, the SLIPI-LIF/Mie signal detection setup is equipped with a 135 mm objective (Pentagon 2.8/135), a beam cube splitter, two optical filters, and two identical sCMOS. However, camera position 2 of the (macroscopic) SLIPI-LIF/Mie detection is at a distance of 915 mm between the objective lens and the light sheet compared to a distance of 225 mm in the case of camera position 1 for the macroscopic LIF/Mie setup. The observed variation in LIF/Mie ratio for camera positions 1 and 2 is not significant (less than 2.5%; not shown here, see [40]). The injector is a five-hole solenoid DISI injector (BOSCH GmbH, Germany) as given in Fig. 2. The diameter of the holes is 168 μm, and the length to diameter ratio (L/D) is 1.7. Here, one jet is centrally separated from the others allowing unrestricted optical access (see normal view). The side view and the bottom view show all five spray plumes. Section A-A, which is 20 mm below the nozzle tip, shows the spray interaction of the neighboring

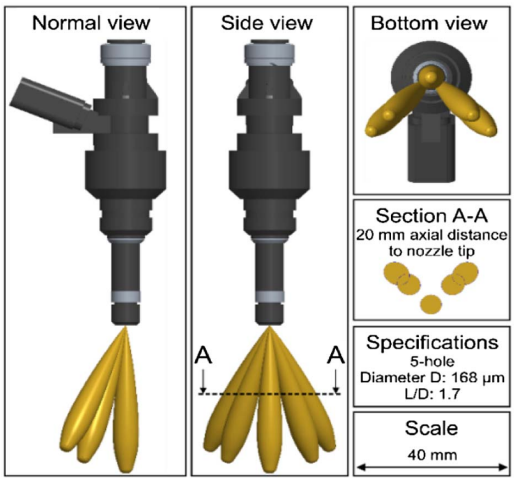


**Fig. 2.** Schematic of the five-hole DISI injector specifications along with the possible spray targeting regions.

plumes. The liquid injection pressure is set to 16 MPa, while the CVC chamber is operated with dry air at 0.2 MPa pressure and 298 K temperature.

For 3D reconstruction of the spray, it is sectioned radially (along the $z$ direction; see also Fig. 6) using the SLIPI light sheet. To that end, the spray system is mounted on a translational stage, and it is moved while keeping the light sheet and camera system fixed. For the comparison of droplet SMD measured with SLIPI-SMD, an independent PDA measurement system is utilized to analyze droplet sizes in the spray. The system consists of a PDA receiver (FiberPDA) and a PDA transmitter (FiberFlow) from Dantec Dynamics A/S, Denmark. To create a PDA probe volume, a pair of two beams of wavelengths 476.5 nm and 514.5 nm is used. The resulting probe volume (length: 468 µm × width: 45 µm) contains 15 fringes with a fringe spacing of about 2.67 µm. This setup leads to a measurement range of droplet sizes up to 50 µm. The signal detection is performed at a Brewster angle of 70° to minimize the effects of refractive index changes in the droplet. A maximum of 10,000 droplets is collected for validation of droplet SMD at every measurement point, which corresponds to up to 120 injections. The SMD data are acquired at different locations within the fuel spray, which is between 10–70 mm in axial direction and −5 mm to +5 mm in radial direction (see Fig. 8). This means that the total PDA measurement time for one location is 120 s or 78 min for 39 studied positions (at an injection frequency of 1 Hz). Using the LIF/Mie technique, the same plane can be characterized within 200 s (i.e., 200 injections were studied in this case).

## 4. 2D RESULTS

### A. Calibration of LIF/Mie Ratio Using Single Droplets

Figure 3 shows the macroscopic LIF and Mie images of the ethanol droplets chain in (a) and the resulting calibration curve of LIF/Mie ratio as a function of droplet diameter in (b). The zoomed area on the left side of the LIF image can be seen as bright spots on the right side. However, in the zoomed view of the Mie image, only one glare point (out of two) is distinctly

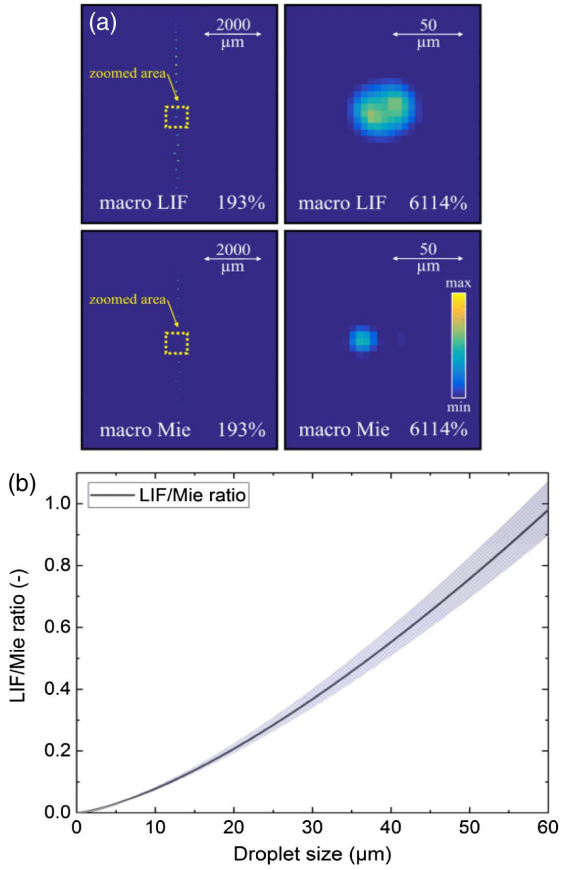


**Fig. 3.** (a) Macroscopic LIF (upper row) and Mie images (bottom row) of ethanol droplet chain of a 48 µm large droplet. (b) Fitting curve of LIF/Mie ratio plotted as a function of droplet diameter of ethanol droplets (0.5 vol% eosin, 293 K). The curves of the standard deviation are given as well.

visible. The zoomed view is presented to demonstrate the setup's ability to resolve the individual signals properly. Note that the simultaneous microscopic measurements used for determination of droplet diameter are presented in [40] along with discussion on the evaluation of single droplet measurement data and morphology-dependent resonance (which has very low impact in this study). In (b), an approximately linear fitting curve of dependence between macro LIF/Mie ratio and droplet diameter is deduced according to Eq. (1), and it can be expressed as

$$R_{\frac{\mathrm{LIF}}{\mathrm{Mie(macro)}}} = 0.0030 \cdot d_{\mathrm{droplet}}^{1.41} \tag{2}$$

The macroscopic LIF/Mie ratio calibration curve of Eq. (2) is utilized because of its large field-of-view imaging of droplets, which is similar to the planar droplet sizing in sprays. The uncertainty of the calibration data based on standard deviation is plotted as well. Here, the $(1-\sigma)$ uncertainties are deduced, resulting approximately in the range of 5.5% for a droplet size of 30 µm. The pre-factor (A) is 0.0030, and the geometric standard deviation is 1.0445, while the exponent (b) is 1.4139, and the corresponding geometric standard deviation is 0.0115. These calculations are described in detail in [40].

### B. Instantaneous Images of DISI Sprays

Figure 4 shows the instantaneous LIF, Mie, and their corresponding ratio images of ethanol DISI spray. These images are recorded at 2552 μs after the visible start of injection (aVSOI). The LIF/Mie ratio is higher near the spray edges and spray front, which is similar to data presented in [23]. It should be noted that the operating point in this publication is different compared to previous studies (injection pressure was 8 MPa in [23] and here it is 16 MPa). The LIF/Mie ratio is converted to instantaneous absolute SMD maps using the calibration curve in Fig. 3(b). The instantaneous images of absolute SMD in Fig. 5 demonstrate the variations in spray structure from one injection to another. The SMD of droplets is mainly in the size range of 5–40 μm between 20–60 mm distances from the nozzle tip. At the spray front between 60–75 mm, the droplet size ranges from 30 μm to 50 μm. The SMD values between 0 mm and 20 mm below the nozzle should not be considered in this evaluation due to the presence of deformed droplets and ligaments, which violates the PDS hypothesis of spherical droplets. The cyclic variations in the spray structure appear mostly near the spray front and at radial spray, boundaries (also see the coefficient of variation (COV) in Fig. 11). Larger vortices appear at the radial edges of the spray, but they are of different size and are not symmetrically distributed.

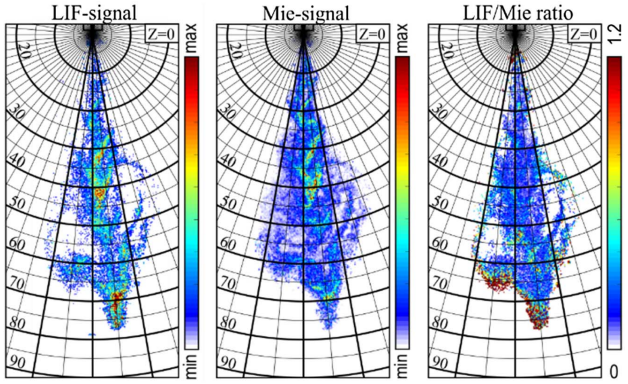


**Fig. 4.** Instantaneous images of LIF, Mie, and corresponding LIF/Mie ratio for ethanol DISI spray at 2552 μs aVSOI.

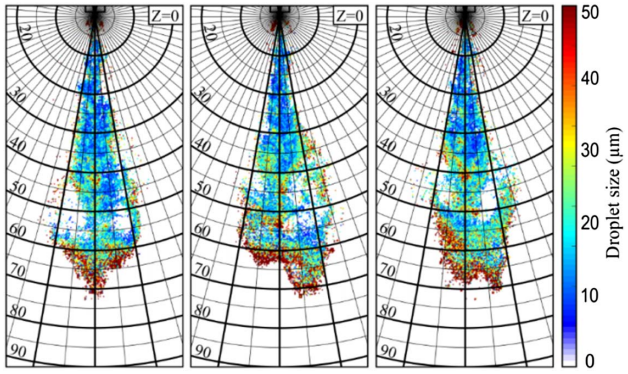


**Fig. 5.** Instantaneous absolute SMD maps in ethanol DISI sprays at 2552 μs aVSOI. The regions between $y = 20$–$60$ mm below the nozzle exit show droplet sizes in the range of 5–45 μm. In the regions between $y = 60$–$75$ mm, the droplet SMD ranges from 20–50 μm.

### C. Averaged SMD Images of DISI Sprays

Figure 6 shows the averaged 2D maps of droplet SMD at different layers of the spray along the $z$ direction between $-8$ mm $\leq z \leq +10$ mm. A total of 51 such layers is recorded with a step size of 0.5 mm along the $z$ axis (for $z = -10$ mm to $+15$ mm; see also Section 5). Each layer represents an averaged distribution of 200 instantaneous images (see Fig. 5), which are sufficient for averaged representation (also in the offset plane $z = +10$ mm, at least 100 images contain SMD data). The average droplet SMD varies between a minimum of about 1 μm and a maximum of 30 μm. The layer-wise 2D maps give better insight of the droplet size distribution through the 3D volume of DISI sprays. At first glance, it is obvious that the spray does not appear symmetric. The spray is illuminated by only one laser light sheet that enters the chamber from the left side. However, in the average droplet size maps, no distinct systematic signal extinction is visible. This indicates that there must be physical reasons in the spray formation process leading to the asymmetric spray.

Interestingly, in the central plane $z = 0$ mm, the maximum droplets are about 25 μm, while in the slices $z = -4$ mm and $z = -6$ mm, larger droplets (~30 μm) appear at the spray front. Apparently, the spray axis is bent towards $z = -4$ mm, and due to the bending of this jet, spray deviates from the original spray targeting. In general, this is an averaged bending, which is different from injection to injection, and this cyclic variation in spray shape is also visible in Fig. 5. There, the spray is sometimes bent more to the left or to the right, while sometimes larger recirculation zones appear at one side, which push the spray in the opposite direction. These vortices and the general spray fluctuations are generated by spray-induced turbulence in the chamber and also by the highly unsteady, cavitating nozzle flow (which leads to variations in the cone angle and bent angle already in the near-nozzle region) [43]. Furthermore, the individual jet may be additionally bent due to jet-to-jet interactions. For example, in the planes $z = -8$ mm to $z = 0$ mm, two more jets of the multi-hole injector

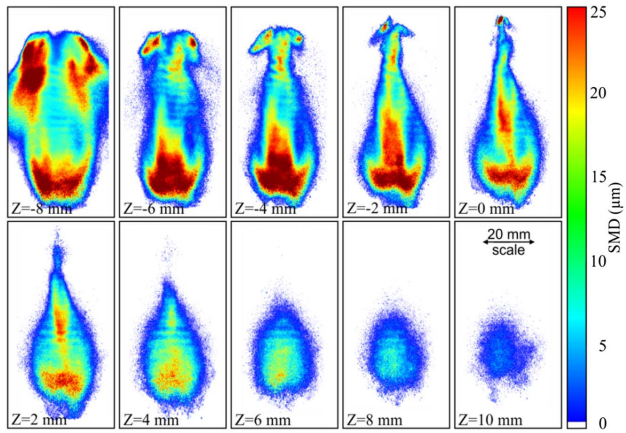


**Fig. 6.** Averaged absolute SMD maps of droplet in ethanol DISI sprays at different $z$ planes between $z = -8$ mm to $z = 10$ mm. Recording time is at 2552 μs aVSOI.

are visible at the left and right sides of the central jet. These interactions could contribute to the deviation from the defined spray targeting as well, which also occurs under some conditions for this injector; see [44]. This issue is discussed further in Section 5.

Additionally, it is important to mention that there are some residual lines on all the 2D slices in Fig. 6. Those are artifacts created due to the field-dependent intensity fluctuation in between the two modulated sub-images. In some situations, the second sub-image ($I_{180}$) has a higher amplitude of the modulation than the first sub-image ($I_0$), despite the correction for light intensity fluctuations as demonstrated in [45]. These residuals are more pronounced in the averaged images compared to those of single-shot images shown in Fig. 5, where residuals are not visible.

### D. Comparison Between SLIPI-SMD and PDA-SMD

A comparison of 2D SMD extracted from SLIPI LIF/Mie and droplet calibration (at $z = 0$ mm, in Fig. 7) is performed with point-wise SMD acquired from PDA measurements. Figure 8 shows the PDA measurement locations throughout the spray region (left side), and data very close to the nozzle tip are not plotted, as SMD measured by SLIPI-LIF/Mie in this region is not considered due to the presence of irregular ligaments (that disappear after a few 100 μm) and non-spherical drops (that exist due to secondary breakup and droplet coalescence further downstream). Thus, only the measurement points at a distance below 40 mm from the nozzle tip are compared. The SMD distribution of the PDA and SLIPI-LIF/Mie has been found overall in a good agreement, along both the radial distance (−5 mm to +5 mm) and the axial distance (40 mm–75 mm). It can be seen that larger droplets exist around the spray central axis and at the spray front (up to 25 μm in the mean image, while maximum droplets are up to 50 μm in the single images as shown above). The smallest droplets at the radial edges are in the range of a few μm. Although the trends of the SMD distributions are similar for PDA and SLIPI-LIF/Mie, still distinct deviation of the local SMD is visible. When considering the measurement points along the injector axis ($z = 0$, $y = 0$ mm) for $x = 40$ mm to 60 mm, the deviations are between 11% and 39% (27% on average). The spray front is not considered, as fewer droplets are collected for the respective time period (PDA data are measured continuously in time, but for determination of the SMD, droplet sizes are averaged over a ±50 μs period). Similarly, in [23], average deviations of 12%–14% occurred, although the LIF/Mie technique was also calibrated with PDA data, which were recorded in the same spray. In principle, a major uncertainty is introduced by the PDA measurements [23], which is in the range of at least 4% in spray the SLIPI-SMD and PDA-SMD overlaid (right side) together. The PDA areas are without significant multiple scattering [15]. This value is expected to be much larger in the present spray.

Another source of error is introduced by the calibration of the LIF/Mie ratio technique using the droplet generator. The $1-\sigma$ uncertainty of the single droplet calibration data reported in [40] is about 5.5% for droplet sizes of 30 μm at 293 K. Additionally, droplet temperature changes of about 10 K could occur in the present spray due to evaporation, which would result in an uncertainty of 4%. Probably, the largest error is set forth by the increasing dye concentration during (weak) evaporation of the spray. It is expected that an increase in dye concentration in the droplets of less than 10% occurs, which corresponds to an uncertainty in droplet sizing of about 6.7%. These uncertainties are explained in detail in [40]. Overall, this would result in an uncertainty of about 9.5% (propagation of uncertainty) for the calibration.

The above presented 2D images are further used to reconstruct a 3D map of droplet SMD (see Figs. 8 and 9). With that 3D reconstruction, it is possible to analyze the real spray structure in comparison to the adjusted targeting by the nozzle holes. Furthermore, the jet-to-jet interactions (which are obvious in layer $z = -8$ mm, but not in layer $z = 0$ mm) can be worked out. This results as the intersection and merging of individual jets, which may lead to collisions and coalescence of droplets from different jets and, therefore, the formation of large droplets in that region.

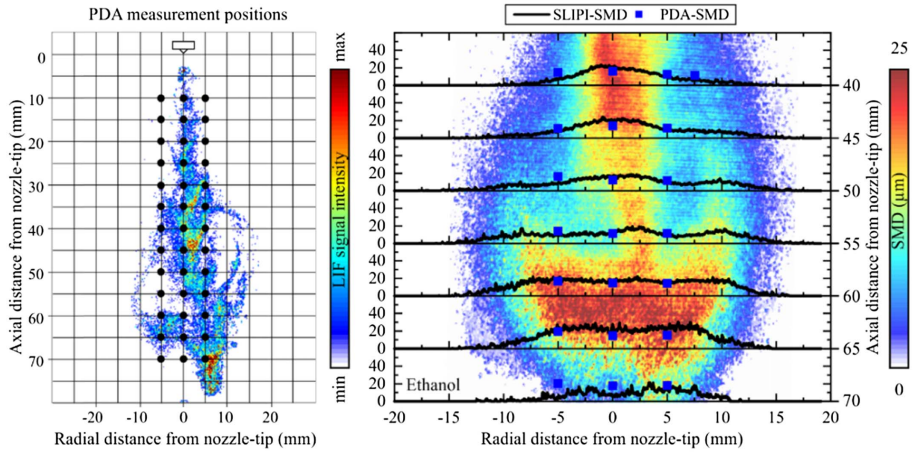


**Fig. 7.** PDA measurement points throughout the spray image (left side) and SLIPI-SMD and PDA-SMD overlaid together (right side) for the central plane ($z = 0$ mm). Recording time is at 2552 μs aVSOI.

## 5. 3D RESULTS

The averaged 3D SMD maps of ethanol DISI sprays are given in Figs. 8 and 9. These are reconstructed from a total of 51 ($z = -10$ mm to $+15$ mm) individual 2D layers of droplet SMD (see Fig. 6). It is seen that 3D maps provide a global representation of droplet SMD in ethanol DISI sprays for the size range of about 1–30 μm. In Fig. 8, several views (side left, side right, front (starting at $z = +15$ mm) and back (starting at $z = -10$ mm) of the 3D reconstruction are shown along with the visualization of the spray in the CVC. This representation explains that not the full volume of spray is accessible due to the relatively small windows (length: 140 mm, clear width: 40 mm), i.e., the front and back views are clipped at the left and right while the back view ends at $z = -10$ mm. The central dotted line denotes the axis of the injector and initial spray from which the bending of the spray can be assessed. In Fig. 9, the back view of the 3D reconstructions of DISI sprays is provided with different SMD ranges of droplet distribution from 20–30 μm (left image), 10–20 μm (middle), and 1–10 μm (right image). These images provide better insight into the inner structure of the investigated spray.

The droplet sizes at the spray edges are mainly in the range of 1–10 μm, while the droplets within the spray cone are in the range of 10–30 μm. The droplets at the spray front and along the spray axis are in the range of 20–30 μm, which is caused mainly by a droplet coalescence mechanism. Furthermore, larger SMDs exist close to the nozzle, especially for the other four jets that show stronger interactions and distinct droplet coalescence (see the schematic of the spray targeting in Fig. 2). The determined droplet sizes are in the range common for DISI-engine sprays.

Figures 10 and 11 show axial and radial cross sections of the averaged droplet SMD and the corresponding COV maps, respectively. First, the 2D map of the middle plane at the axial distance $z = 0$ mm and the radial distance of $x = 20$–$90$ mm is shown. Then the six cross sections of the spray, at $x = 20$–$70$ mm for $z = -10$ mm to $+15$ mm are shown for both SMD and COV. The COV maps in Fig. 11 show the cyclic

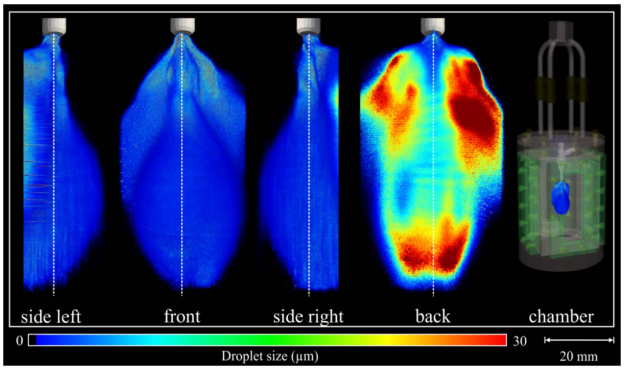


**Fig. 8.** Side left, front, side right, and back views of the reconstructed 3D maps of droplet SMD for ethanol DISI spray. The visualization of the spray in the constant volume chamber is shown in the right image.

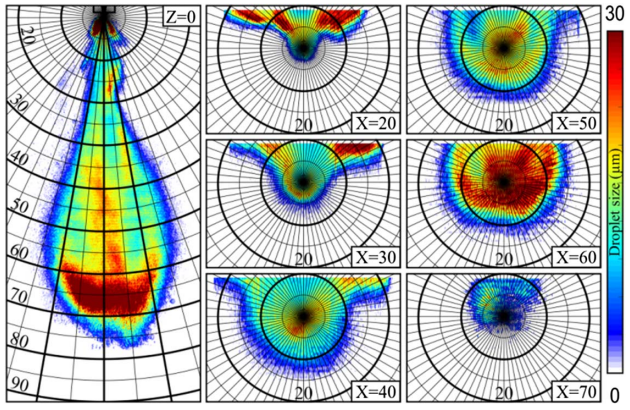


**Fig. 10.** Averaged absolute SMD cross-section maps of DISI spray. Droplet SMD ranges from about 1 μm to 30 μm. Recording time is at 2552 μs aVSOI.

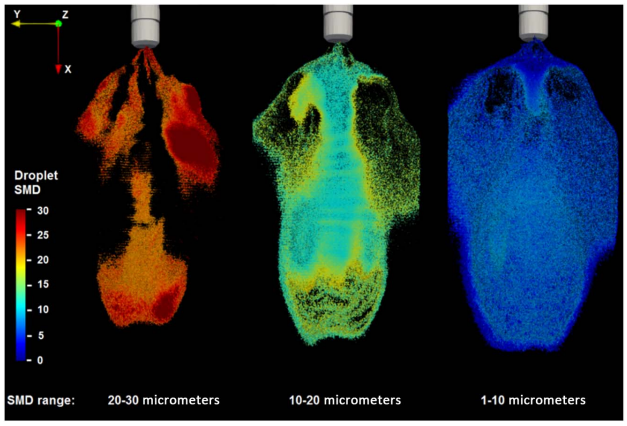


**Fig. 9.** Back view: 3D map of the DISI spray plotted as a function of droplet SMD range, for better insight into the inner structure of the spray: 20–30 μm (left), 10–20 μm (middle), and 1–10 μm (right).

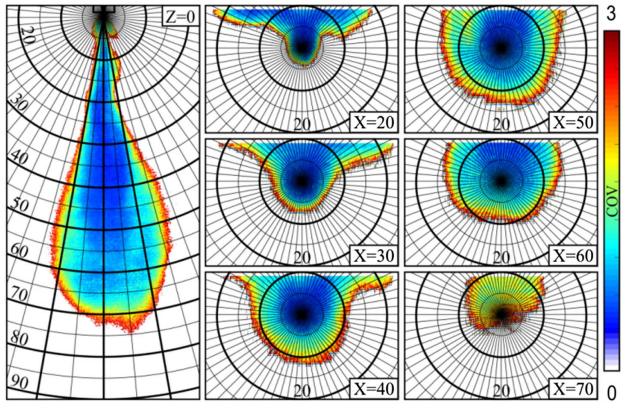


**Fig. 11.** COV of SMD cross-section maps for ethanol DISI sprays. The COV maps show strong cyclic variations near the spray edges and spray front. Recording time is at 2552 μs aVSOI.

variability of the SMD in the sprays. The COV increases near the spray edges and spray front in accordance with distinct cyclic variations of the spray shape in these regions observed in the single-shot images (see Fig. 5).

It is evident from the images that the spray is not symmetric to the injector axis, especially in regions 30–70 mm from the nozzle, while this asymmetry increases with larger distance from the nozzle tip, and that a single central plane in the axial direction is not representative to analyze the spray structure. A distinct jet-to-jet interaction is visible in the planes $x = 20$ mm to $x = 40$ mm, as three jets (or actually all five jets in the plane $x = 20$ mm) are clearly merged. This leads to much larger droplets in the intersecting regions.

Furthermore, the central jet is drawn towards the other jets, which is visible mainly in planes $x = 60$ mm and $x = 70$ mm, where the center of the jet axis moves about 5 mm away from the injector axis (which is indicated by the intersection of all black lines of the grid). This confirms that a contraction of the whole spray results also under the studied injection conditions due to the spray-induced low-pressure field between these jets. This spray contraction would be even stronger for very low ambient pressure conditions (less than 0.1 MPa) that support flash boiling [44,46]. Furthermore, in planes $x = 50$ mm and $x = 60$ mm, the position and the shape of the vortices is visible. Inside the recirculation zones, the droplet size is smaller compared to the surrounding spray regions. Again, the average vortices are not symmetrically distributed around the spray, and larger droplets are situated at the rightedge of the spray. At this side, the axial penetration is also increased, which correlates with the larger momentum due to the higher droplet mass in that region. Larger droplets are also apparent in the planes $x = 30$ mm and $x = 40$ mm at the right edge of the jet adjacent to the neighboring jet, which is probably due to stronger jet-to-jet interactions and droplet collisions in this region.

## 6. CONCLUSION AND OUTLOOK

In conclusion, the light sheet scanning approach based on structured illumination proposed here provides a series of 2D images of droplet SMD from the spray region in optically dense sprays. The 2D images obtained at several $z$ distances can be combined to reconstruct a 3D map of the droplet SMD. The LIF/Mie ratio calibration was performed with single-droplet measurements, and an approximately linear relation between the ratio and droplet diameter was deduced. The SMD distribution of dense sprays extracted from SLIPI-LIF/Mie ratio and from the PDA measurements were found overall in a good agreement. The averaged droplet SMD of ethanol DISI sprays were in the range of about 1–30 μm, while single-shot images showed SMD of up to 50 μm. The single-shot images and COV map showed strong cyclic variation in multi-jet DISI spray near the spray edges and spray fronts. Through the approach presented, it was possible to study the inner structure of the optically dense spray over a large volume in terms of SMD. This analysis showed an asymmetric spray structure deviating from its initial targeting, as the jets overlap and are drawn together further downstream from the nozzle. In the future, the limitations of the LIF/Mie ratio approach for optically denser sprays will be investigated.

**Funding.** German Federal Ministry of Food and Agriculture (BMEL) through the Agency for Renewable Resources (FNR), FKZ: 22026711; Deutsche Forschungsgemeinschaft (DFG); H2020 European Research Council (ERC) under the European Union's Horizon 2020 research and innovation program (Agreement No. 638546-ERC starting grant "Spray-Imaging").

**Acknowledgment.** Erlangen Graduate School in Advanced Optical Technologies (SAOT), which is funded by the German Research Foundation (DFG). We thank Bernd Eppinger for supporting the experiments.

## REFERENCES

1. N. Chigier, "An assessment of spray technology—editorial," Atomization Sprays **3**, 365–371 (1993).
2. K. Lee and J. Abraham, "Spray applications in internal combustion engines," in *Handbook of Atomization and Sprays: Theory and Applications*, N. Ashgriz, ed., (Springer, Boston, MA, 2011), pp. 777–810.
3. N. Kawahara, E. Tomita, H. Nakasuji, and M. Sumida, "PDA measurement of transient spray formed by a DISI multi-hole injector," in *10th International Conference on Liquid Atomization and Spray Systems* (Kyoto, 2006).
4. L. Zigan, I. Schmitz, A. Flügel, T. Knorsch, M. Wensing, and A. Leipertz, "Effect of fuel properties on spray breakup and evaporation studied for a multihole direct injection spark ignition injector," Energy Fuels **24**, 4341–4350 (2010).
5. S. Lee, Y. Oh, and S. Park, "Characterization of the spray atomization process of a multi-hole gasoline direct injector based on measurements using a phase Doppler particle analyser," Proc. Inst. Mech. Eng. D **227**, 951–965 (2013).
6. G. Wigley, M. Goodwin, G. Pitcher, and D. Blondel, "Imaging and PDA analysis of a GDI spray in the near-nozzle region," Exp. Fluids **36**, 565–574 (2004).
7. C. N. Yeh, H. Kosaka, and T. Kamimoto, "Fluorescence/scattering image technique for particle sizing in unsteady diesel spray," Trans. Jpn. Soc. Mech. Eng. B **59**, 4008–4013 (1993).
8. W. Zeng, M. Xu, Y. Zhang, and Z. Wang, "Laser sheet dropsizing of evaporating sprays using simultaneous LIEF/MIE techniques," Proc. Combust. Inst. **34**, 1677–1685 (2013).
9. A. Malarski, B. Schürer, I. Schmitz, L. Zigan, A. Flügel, and A. Leipertz, "Laser sheet dropsizing based on two-dimensional Raman and Mie scattering," Appl. Opt. **48**, 1853–1860 (2009).
10. S. Bareiss, B. Bork, S. Bakić, C. Tropea, R. Irsig, J. Tiggesbäumker, and A. Dreizler, "Application of femtosecond lasers to the polarization ratio technique for droplet sizing," Meas. Sci. Technol. **24**, 025203 (2013).
11. R. Wellander, E. Berrocal, E. Kristensson, M. Richter, and M. Aldén, "Three-dimensional measurement of the local extinction coefficient in a dense spray," Meas. Sci. Technol. **22**, 125303 (2011).
12. C. N. Yeh, H. Kosaka, and T. Kamimoto, "A fluorescence/scattering imaging technique for instantaneous 2-D measurements of particle size distribution in a transient spray," in *Proceedings of the 3rd Congress on Optical Particle Sizing*, Japan (1993), pp. 355–361.
13. P. Le Gal, N. Farrugia, and D. A. Greenhalgh, "Laser sheet dropsizing of dense sprays," Opt. Laser Technol. **31**, 75–83 (1999).
14. K. Kannaiyan, M. V. K. Banda, and A. Vaidyanathan, "Planar Sauter mean diameter measurements in liquid centered swirl coaxial injector using laser induced fluorescence, Mie scattering and laser diffraction techniques," Acta Astronaut. **123**, 257–270 (2016).
15. M. C. Jermy and D. A. Greenhalgh, "Planar dropsizing by elastic and fluorescence scattering in sprays too dense for phase Doppler measurement," Appl. Phys. B **71**, 703–710 (2000).
16. R. Domann and Y. Hardalupas, "A study of parameters that influence the accuracy of the planar droplet sizing (PDS) technique," Part. Part. Syst. Charact. **18**, 3–11 (2001).

17. R. Domann and Y. Hardalupas, "Quantitative measurement of planar droplet Sauter mean diameter in sprays using planar droplet sizing," Part. Part. Syst. Charact. **20**, 209–218 (2003).
18. B. D. Stojkovic and V. Sick, "Evolution and impingement of an automotive fuel spray investigated with simultaneous Mie/LIF techniques," Appl. Phys. B **73**, 75–83 (2001).
19. S. Park, H. Cho, I. Yoon, and K. Min, "Measurement of droplet size distribution of gasoline direct injection spray by droplet generator and planar image technique," Meas. Sci. Technol. **13**, 859–864 (2002).
20. S. H. Jin, M. Brear, H. Watson, and S. Brewster, "An experimental study of the spray from an air-assisted direct fuel injector," Proc. Inst. Mech. Eng. D **222**, 1883–1894 (2008).
21. A. A. Boretti, S. H. Jin, G. Zakis, M. J. Brear, W. Attard, H. Watson, H. Carlisle, and W. Bryce, "Experimental and numerical study of an air assisted fuel injector for a D.I.S.I. engine," SAE Technical Paper 2007–01–1415 (2007).
22. M. Storch, Y. N. Mishra, M. Koegl, E. Kristensson, S. Will, L. Zigan, and E. Berrocal, "Two-phase SLIPI for instantaneous LIF and Mie imaging of transient fuel sprays," Opt. Lett. **41**, 5422–5425 (2016).
23. M. Koegl, Y. N. Mishra, M. Storch, C. Conrad, E. Berrocal, S. Will, and L. Zigan, "Analysis of ethanol and butanol direct-injection spark-ignition sprays using two-phase structured laser illumination planar imaging droplet sizing," Int. J. Spray Combust. Dyn., 1756827718772496 (2018).
24. G. Charalampous and Y. Hardalupas, "Method to reduce errors of droplet sizing based on the ratio of fluorescent and scattered light intensities (laser-induced fluorescence/Mie technique)," Appl. Opt. **50**, 3622–3637 (2011).
25. G. Charalampous and Y. Hardalupas, "Numerical evaluation of droplet sizing based on the ratio of fluorescent and scattered light intensities (LIF/Mie technique)," Appl. Opt. **50**, 1197–1209 (2011).
26. R. Domann, Y. Hardalupas, and A. R. Jones, "A study of the influence of absorption on the spatial distribution of fluorescence intensity within large droplets using Mie theory, geometrical optics and imaging experiments," Meas. Sci. Technol. **13**, 280–291 (2002).
27. B. Frackowiak and C. Tropea, "Fluorescence modeling of droplets intersecting a focused laser beam," Opt. Lett. **35**, 1386–1388 (2010).
28. B. Frackowiak and C. Tropea, "Numerical analysis of diameter influence on droplet fluorescence," Appl. Opt. **49**, 2363–2370 (2010).
29. E. Berrocal, I. Meglinski, and M. Jermy, "New model for light propagation in highly inhomogeneous polydisperse turbid media with applications in spray diagnostics," Opt. Express **13**, 9181–9195 (2005).
30. D. Stepowski, O. Werquin, C. Roze, and T. Girasole, "Account for extinction and multiple scattering in planar droplet sizing of dense sprays," in *13th International Symposium of Laser Techniques to Fluids Mechanics*, Lisbon (2006), paper 1061.
31. J. W. Powell and C.-f. F. Lee, "An investigation of multiple scattering in a hollow-cone spray," SAE Technical Paper 2007–01–0648 (2007).
32. E. Berrocal, E. Kristensson, M. Richter, M. Linne, and M. Aldén, "Application of structured illumination for multiple scattering suppression in planar laser imaging of dense sprays," Opt. Express **16**, 17870–17881 (2008).
33. E. Kristensson, E. Berrocal, M. Richter, S. G. Pettersson, and M. Aldén, "High-speed structured planar laser illumination for contrast improvement of two-phase flow images," Opt. Lett. **33**, 2752–2754 (2008).
34. E. Berrocal, E. Kristensson, P. Hottenbach, M. Aldén, and G. Grünefeld, "Quantitative imaging of a non-combusting diesel spray using structured laser illumination planar imaging," Appl. Phys. B **109**, 683–694 (2012).
35. Y. N. Mishra, E. Kristensson, and E. Berrocal, "3D droplet sizing and 2D optical depth measurements in sprays using SLIPI based techniques," in *18th International Symposium on the Application of Laser and Imaging Techniques to Fluid Mechanics*, Lisbon (2016).
36. Y. N. Mishra, E. Kristensson, and E. Berrocal, "Reliable LIF/Mie droplet sizing in sprays using structured laser illumination planar imaging," Opt. Express **22**, 4480–4492 (2014).
37. A. P. Kulkarni and D. Deshmukh, "Improvements in laser sheet dropsizing using numerical and experimental techniques," Int. J. Multiphase Flow **110**, 273–281 (2019).
38. S. Bareiss, N. Fuhrmann, A. Dreizler, H. Bacher, J. Höffner, R. Weishäupl, and D. Kügler, "Planar droplet sizing for characterization of automotive sprays in port fuel injection applications using commercial fuel," in *Flow and Combustion in Advanced Gas Turbine Combustors* (Springer Netherlands, 2013), pp. 445–461.
39. H. Duan, F. Romay, Z. Syedain, B. Y. H. Liu, and A. Naqwi, "A new monodisperse droplet generator and its applications," in *28th Annual Conference on Liquid Atomization and Spray Systems*, Dearborn (2016).
40. M. Koegl, B. Hofbeck, K. Baderschneider, Y. N. Mishra, F. J. T. Huber, E. Berrocal, S. Will, and L. Zigan, "Analysis of LIF and Mie signals from single micrometric droplets for instantaneous droplet sizing in sprays," Opt. Express **26**, 31750–31766 (2018).
41. R. A. Mugele and H. D. Evans, "Droplet size distribution in sprays," Indust. Eng. Chem. **43**, 1317–1324 (1951).
42. H. Chen, M. Xu, W. Zeng, M. Zhang, G. Zhang, and Y. Zhang, "An improved monosize droplet generator for SMD calibration," in *13th Annual Conference on Liquid Atomization and Spray Systems*, Wuxi (2009).
43. L. Zigan, J. M. Shi, I. Krotow, I. Schmitz, M. Wensing, and A. Leipertz, "Fuel property and fuel temperature effects on internal nozzle flow, atomization and cyclic spray fluctuations of a direct injection spark ignition-injector," Int. J. Engine Res. **14**, 543–556 (2013).
44. M. Heldmann, S. Bornschlegel, and M. Wensing, "Investigation of Jet-to-Jet Interaction in Sprays for DISI Engines," SAE Technical Paper 2015-01-1899 (2015).
45. Y. N. Mishra, E. Kristensson, M. Koegl, J. Jönsson, L. Zigan, and E. Berrocal, "Comparison between two-phase and one-phase SLIPI for instantaneous imaging of transient sprays," Exp. Fluids **58**, 110 (2017).
46. M. Krämer, E. Kull, and M. Wensing, "Flashboiling-induced targeting changes in gasoline direct injection sprays," Int. J. Engine Res. **17**, 97–107 (2016).